

## Article

# Evaluation of Bone Consolidation in External Fixation with an Electromechanical System

Maria F. Paulino <sup>1,\*</sup> , Luis M. Roseiro <sup>1,2</sup> , Inês Balacó <sup>3</sup>, Maria A. Neto <sup>1</sup>  and Ana M. Amaro <sup>1</sup> 

<sup>1</sup> Department of Mechanical Engineering, Center for Mechanical Engineering, Materials and Processes (CEMMPRE), University of Coimbra, 3030-788 Coimbra, Portugal; lroseiro@isec.pt (L.M.R.); augusta.neto@dem.uc.pt (M.A.N.); ana.amaro@dem.uc.pt (A.M.A.)

<sup>2</sup> Polytechnic of Coimbra, ISEC, Rua Pedro Nunes—Quinta da Nora, 3030-199 Coimbra, Portugal

<sup>3</sup> Pediatric Orthopedics Service of the Pediatric Hospital of Coimbra—CHUC, EPE, 3004-561 Coimbra, Portugal; inesbalaco@gmail.com

\* Correspondence: maria.paulino@dem.uc.pt; Tel.: +351-239-790-700

**Featured Application:** The findings of this work can help doctors decide when it is appropriate to remove the external fixator.

**Abstract:** The monitoring of fracture or osteotomy healing is vital for orthopedists to help advise, if necessary, secondary treatments for improving healing outcomes and minimizing patient suffering. It has been decades since osteotomy stiffness has been identified as one main parameter to quantify and qualify the outcome of a regenerated callus. Still, radiographic imaging remains the current standard diagnostic technique of orthopedists. Hence, with recent technological advancements, engineers need to use the new branches of knowledge and improve or innovate diagnostic technologies. An electromechanical system was developed to help diagnose changes in osteotomy stiffness treated with the external fixator LRS Orthofix<sup>®</sup>. The concept was evaluated experimentally and numerically during fracture healing simulation using two different models: a simplified model of a human tibia, consisting of a nylon bar with a diameter of 30 mm, and a synthetic tibia with the anatomical model from fourth-generation Sawbones<sup>®</sup>. Moreover, Sawbones<sup>®</sup> blocks with different densities simulated the mechanical characteristics of the regenerated bone in many stages of bone callus growth. The experimental measurements using the developed diagnostic were compared to the numerically simulated results. For this external fixator, it was possible to show that the displacement in osteotomy was always lower than the displacement prescribed in the elongator. Nevertheless, a relationship was established between the energy consumption by the electromechanical system used to perform callus stimulus and the degree of osteotomy consolidation. Hence, this technology may lead to methodologies of mechanical stimulation for regenerating bone, which will play a relevant role for bedridden individuals with mobility limitations.

**Keywords:** external fixation; micromovements; bone callus; electromechanical system; bone consolidation



**Citation:** Paulino, M.F.; Roseiro, L.M.; Balacó, I.; Neto, M.A.; Amaro, A.M. Evaluation of Bone Consolidation in External Fixation with an Electromechanical System. *Appl. Sci.* **2022**, *12*, 2328. <https://doi.org/10.3390/app12052328>

Academic Editor: Antonio Scarano

Received: 10 January 2022

Accepted: 16 February 2022

Published: 23 February 2022

**Publisher's Note:** MDPI stays neutral with regard to jurisdictional claims in published maps and institutional affiliations.



**Copyright:** © 2022 by the authors. Licensee MDPI, Basel, Switzerland. This article is an open access article distributed under the terms and conditions of the Creative Commons Attribution (CC BY) license (<https://creativecommons.org/licenses/by/4.0/>).

## 1. Introduction

External fixators are a surgical method of bone immobilization commonly applied to allow a fracture to heal appropriately, providing stability to long bones and soft tissue after a severe fracture. However, they can also be used to protect soft tissues after a burn or severe injury and as a procedure to correct bone misalignment and restore limb length, for example, in the case of dwarfism. The main advantage of external fixation is related to the quickness and facility of its application. Still, because it involves a surgical procedure, it needs to be performed by an orthopedic surgeon. When an external fixation system is applied, the risk of infection at the fracture site is minimal. However, there is some hypothesis that disease may occur at the connection between the rods and the

skin [1]. External fixation systems establish a link in the fragmented bone, allowing load transfer between the parts and promoting interfragmentary movements for bone healing [2]. The interfragmentary movement is the relative movement between the bone fragments, which can appear during a patient's weight-bearing activities. These micromovements in the fracture site are crucial to promoting bone callus growth and the control of bone regeneration [3]. Hence, the controlled physical activity of the patient might represent a mechanical stimulation that contributes to bone healing. Nevertheless, it is also worth stating that excessive mobility would disturb bone consolidation and perturb the healing process, leading to infections and bone misalignments [4–6]. Hence, these interfragmentary movements are crucial for the complex process of consolidating fracture [7].

Nevertheless, mechanical stimulation by patients' weight-bearing activities is only possible in people who can walk. In the case of bedridden patients or of those with reduced mobility, the bone union is more complicated and may even be inhibited by other health problems in the patients that might cause improper or impaired bone healing, leading to a significant increase in treatment time. Hence, all biomechanical devices that can introduce controlled micromovements at the fracture site, contributing to the rehabilitation of patients and reducing the recovery time, are an alternative to help those patients. According to Barcik and Epari [8], the mechanical manipulation of the local fracture environment can significantly decrease fracture patients' healing time, suggesting that additional experiments should be conducted to determine the best parameters. For instance, it is necessary to know when the interfragmentary motion needs to be stopped to allow for consolidation and establish the best stimulation/rest ratio. As radiographic evaluation shows some limitations, several authors are trying to develop methods of healing assessment that can give information about the progression of the mechanical properties of the fracture repair tissue. For example, using implants with sensing capabilities [9,10] or instrumented implants can improve the clinical outcome of total hip replacements [11,12]. These innovative implants can be implementable, provide therapeutic benefits, and have diagnostic capabilities.

Surgical procedures involving bone regeneration and the identification of bone consolidation will help define the exact moment to remove the fixation system. Right now, this identification is assured by equipment having radiation emissions, such as densitometry or tomography. Hence, the development of tools allowing an early identification of the consolidation phase has applicability interest in the scope of patient recovery, particularly for bedridden situations. This study intends to contribute to the introduction of micromovements and the earlier identification of the healing phase of the regenerated bone through an electromechanical system. The presented electromechanical system may also play an essential role in bone stretching, as it can replace the manual introduction made by the patient, automating this process. The prototype was developed in the Orthofix<sup>®</sup> monoplane external fixation system, but the concept can extend to another external fixation type where linear movement might occur.

## 2. Materials and Methods

### 2.1. Experimental Models

This study considered a tibial osteotomy model in the central area of the diaphysis, stabilized using a unilateral external fixator LRS (Limb Reconstruction System), from Orthofix<sup>®</sup> (Munich, Germany), supplied by Orthofix GmbH, Munich, Germany, used in a wide variety of situations. Two experimental models were implemented, one using a synthetic tibia, and another using a single rod representing a simplified tibia geometry [3]. The models did not include soft tissue. Figure 1 illustrates the experimental model set with simplified and anatomical features.

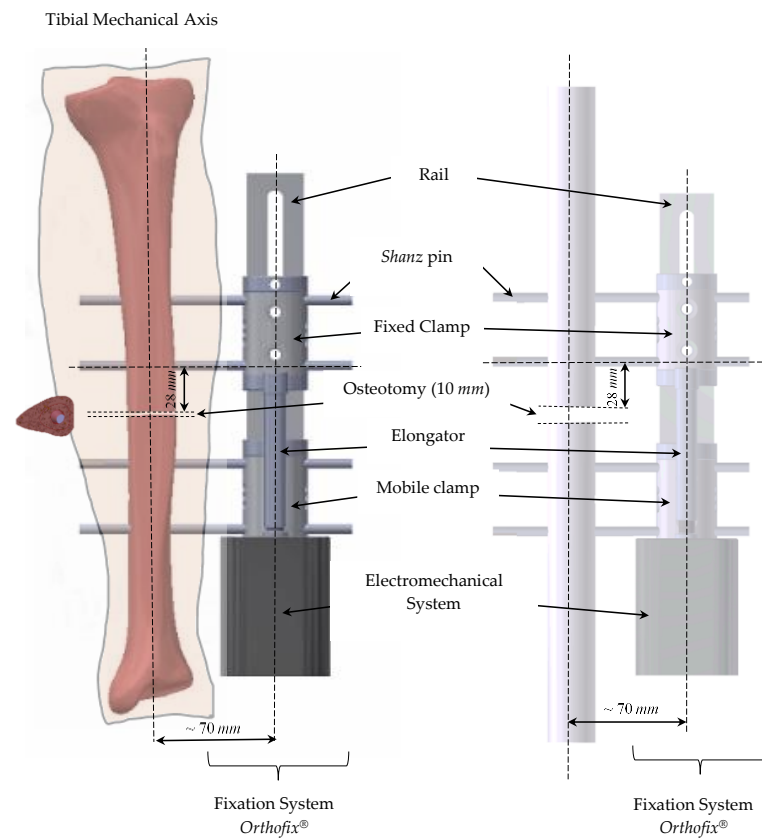


**Figure 1.** Anatomical model/tibial simplified—external fixation.

The anatomical model used a fourth-generation Sawbones<sup>®</sup> tibia, whose geometry has the CAD reference #3401. The model considered the mechanical characteristics of the cortical and trabecular bone as isotropic with the properties given in Table 1. The osteotomy fixation included the LRS unilateral external fixator application and the attached electromechanical system. Schanz pins of 6 mm in diameter and 150 mm in length allowed connecting the fixator to the bone. Schanz pins are produced in AISI 316L steel, and their mechanical properties are shown in Table 1.

**Table 1.** Mechanical properties of cortical and trabecular bone. Mechanical properties of the external fixator.

Designation	Density [kg/m <sup>3</sup> ]	Young Modulus [GPa]	Coefficient of Poisson
Trabecular Bone, [13]	300	0.7	0.20
Cortical Bone, [13]	1800	17.0	0.30
External fixator <i>Orthofix</i> <sup>®</sup> LRS (AISI 7075 T6), [14]	2810	72.0	0.33
<i>Schanz</i> pin (AISI 316L), [14]	8027	200.0	0.27

As shown in Figure 1, the osteotomy was perpendicular to the mechanical axis of the bone, and the two opposite faces were at a distance of 10 mm. The axis of the fixator was 70 mm away from the mechanical axis of the tibia [15,16]. The closest distance from the Schanz pin to the osteotomy was 28 mm. All values were defined according to the indication of the medical team that supported the work.

The electromechanical system presented in Figure 1 includes a motor and an electronic control unit, both placed in a box and coupled to the end of the mobile clamp of the fastener. The worm screw of the elongator is connected to the motor shaft and assures the axial movement of the worm screw. The principal components of the electromechanical system

are presented in Figure 2. The system consists of a micromotor with the reference A-max 16, Maxon® (Sachseln, Suíça), Precious Metal Brushes CLL, 2 Watt, with a 16 mm diameter, which guarantees the axial displacement induction if the mobile clamp is loose, but also the blocking of the movement if required. The micromotor is controlled through a control unit developed on the Arduino® programming platform.

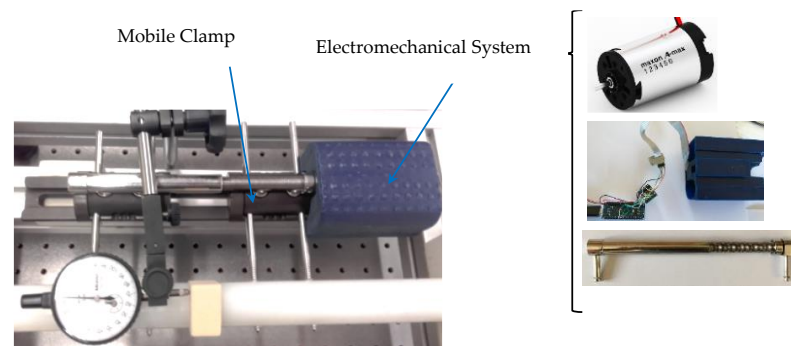


**Figure 2.** Connection of the electromechanical system into the external fixator Orthofix®.

The electromechanical system was powered with a battery and electronically activated using an Encoder MR Type M, 32 CPT, 2/3 Channel for positional control. The hardware systems of the Arduino® board used a DRV8801 plate from Texas Instruments® (Dallas, TX, USA), allowing the bidirectional control of a bridged DC micromotor. The board could supply a direct current up to 1 A, tolerating peak currents that might, for a few seconds, reach values of 2.8 A. Two conductors were needed to power the micromotor to the DRV8801 board, which would receive a voltage of 12 V between the “VMM” e the “GND”. The passage of electric current between the board and the micromotor was assured through the “motor+” e “motor–” pins.

Additionally, an encoder coupled to the micromotor obtained results in the elongator’s instant closing or opening position. The developed software integrates an interface implemented through the Azande® program allowing the user to define some parameters, such as motor speed and position. This program enables the selection of movement type, choosing the linear velocity of the movement, the displacement distance, and the number of repetitions to be performed.

Because the micromotor needed a power supply to ensure the mechanical stimulus, there was also a mechanical resistance, and the motor current consumption was related to the mechanical resistance. Although the resistance depends on several factors, such as the sliding friction among several surfaces, the resistance opposition in the osteotomy mainly contributes to the system’s mechanical resistance. Hence, it is crucial to find a relationship between the rigidity of the osteotomy and the energy to supply to the motor that guarantees the necessary mechanical stimulus. Moreover, after calibration, the electromechanical system creates displacement relationships between the fixator clamp and the osteotomy.

A support platform built-in Aluminum profile of Minitec® (30 × 30) was developed for the two models, allowing the positional adjustment of the components. This structure intended to replicate, in a simplified way, the positioning of the lower limb in the horizontal position, like in a bedridden patient. It included a fixed support, representing the position of knee connection, and a free axial support, which mimicked the relationship with the foot and guided the axial movement introduced in the assembly, as shown in Figure 3. The osteotomy’s displacement was characterized using a Mitutoyo® analogue comparator, with a measurement accuracy of 1 µm and located on one of the faces of Sawbones® block.

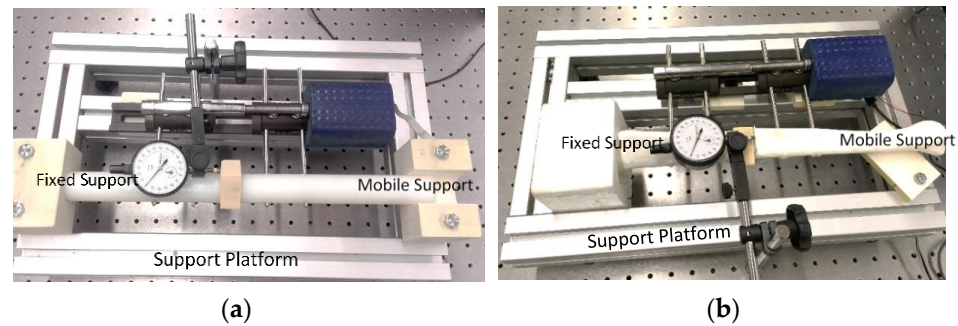


**Figure 3.** Horizontal supporting platform: (a) support conditions of the simplified model; (b) support conditions of the anatomic tibia.

This study used the Sawbones<sup>®</sup> blocks (Sawbones<sup>®</sup>, Malmö, Sweden, 2019) with different densities to simulate different osteotomy rigidities. According to the trademark, these materials allow for a good simulation of the mechanical characteristics of the regenerated bone in the many stages of bone callus growth [17], reproducing the variation in bone callus stiffness. The mechanical properties and the designation of the several materials are in Table 2. This material is applied in osteotomy to carry out advancement tests. These tests are intended to evaluate the resistance capacity of the material when subjected to compression.

**Table 2.** Mechanical properties of the materials used in the osteotomy [18].

Solid Foam	10 PCF	15 PCF	20 PCF	30 PCF	40 PCF	50 PCF
Density [g/cm <sup>3</sup> ]	0.16	0.24	0.32	0.48	0.64	0.80
Tensile Strength [MPa]	2.1	3.7	5.6	12.0	19.0	27.0
Young Modulus (traction) [GPa]	0.086	0.173	0.284	0.592	1.0	1.469
Compressive Strength [MPa]	2.2	4.9	8.4	18.0	31.0	48.0
Young Modulus (Comp.) [GPa]	0.058	0.123	0.210	0.445	0.759	1.148
Coefficient of Poisson	0.3	0.3	0.3	0.3	0.3	0.3

The Sawbones<sup>®</sup> materials have rigidities (stiffness expressed in Young's compression Modulus) between those of fibrous tissue, immature bone, and mature bone. Table 3 compares the Sawbones stiffness values at different densities with bone characteristics in the various phases. Several authors [19,20] used these regenerated bone properties to represent bone regeneration in mathematical models, whereas other researchers created numerical models based on the same information [21–23].

The primary purpose of this experimental setup was to study the relationship between rigidity and micromovements on the osteotomy for the loading conditions defined at the micromotor. Moreover, it was also essential to evaluate the micromotor energy consumption (CEMotor) in forward and backward movements to determine its relationship with the material's stiffness at the osteotomy. Hence, three different displacements were imposed in the osteotomy, corresponding to 1, 1.5, and 2 mm, and, to guarantee repeatability and reproducibility, five tests for each displacement were performed. Several authors argue that the recovery time can be reduced if osteotomy stimulation is promoted with displacements of 1 mm/day [13,24–29].

**Table 3.** Stiffness of the material used to represent osteotomy/regenerative bone [18,20].

	Stiffness [MPa]	
Fibrous Tissue	0.2	
<i>Sawbones</i> <sup>®</sup> 10	58	
<i>Sawbones</i> <sup>®</sup> 15	123	
<i>Sawbones</i> <sup>®</sup> 20	210	
<i>Sawbones</i> <sup>®</sup> 30	445	
<i>Sawbones</i> <sup>®</sup> 40	759	→Stimulation
Immature Bone	1000	
<i>Sawbones</i> <sup>®</sup> 50	1148	
Mature Bone	6000	
Cortical Bone	20,000	

The experimental results are presented using the following notation:

$$\{PA6 ; AN\} S_i v_j d_k \quad (1)$$

where *PA6* represents the simplified model's results, and *AN* those of the anatomical model. The index *i* represents the type of *Sawbones*<sup>®</sup> material, i.e., 10, 20, 30, 40, and 50, the index *j* identifies the speed imposed on the micromotor (2 mm/min), and the index *k* is related to the level of displacement set, i.e., 1 mm, 1.5 mm, and 2 mm.

## 2.2. Numerical Models

The geometrical models were created based on the experimental simplified and anatomical models. Each one of the two model files was imported into the ADINA System for linear and nonlinear finite element analysis (ADINA AUI version 9.3.1, ADINA R&D Inc., Water-town, NY, USA). Figure 4 illustrates the external fixation models that replicate the experimental conditions. Since these models were based on the stimulation concept performed on patients with reduced mobility, the boundary conditions mimicked these physical limitations. Hence, the main movement restrictions were in the knee area, while the support in the foot was less restrictive, and the displacement loading condition was assured at the mobile clamp. Figure 4 also shows the numerical boundary conditions. The three translational degrees of freedom in the tibia condyles regions and the displacements in the *XX* and *ZZ* axis in the foot area were restricted, allowing only axial movement.

The contact among surfaces ensured the material continuity between the faces of the bone and the faces of the osteotomy material, between the pin surfaces and the inner surfaces of the hole bone. Even knowing that the fixation of the clamp to the rail was assured through a screw, the bonded contact allowed simplifying the numerical model. Material continuity guaranteed the connection between the pins and the clamps. The relative movement among the faces involved on the remaining contacts was included. Figure 5 shows the several contact surfaces of the numerical models.

A mesh sensitivity study was assured, assuming that grid displacement independence was achieved for variations in the order of 5%. Assignment of the mesh density to the several bodies of each model was supported by equally spaced subdivisions of the bodies, using the desired edge length dimensions between 1 mm e 3 mm. In some cases, the subdivision of specific faces was recalculated with smaller sizes to assure a more refined mesh in areas requiring higher precision of the results. The Delaunay free-form meshing algorithm guaranteed discretization of the domains, generating an eight-node hexahedral element. Additional displacement degrees of freedom were allowed by selecting the incompatible modes option. The total number of nodes and elements of each model are detailed in Table 4.

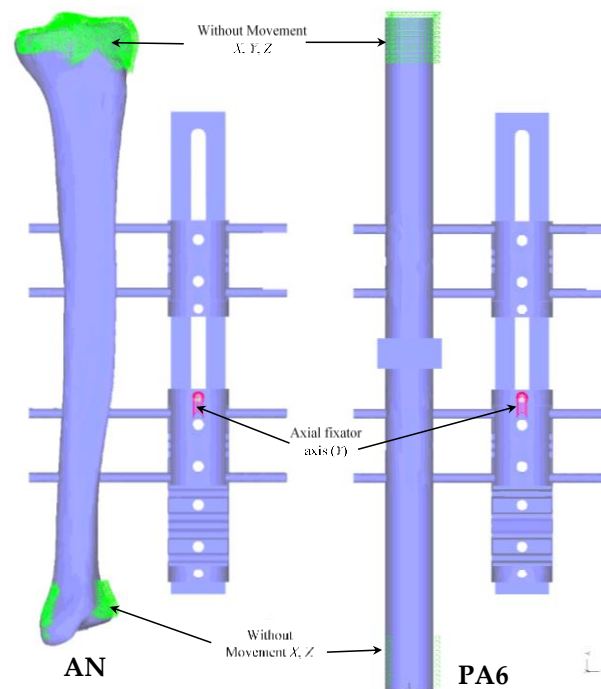


**Figure 4.** Finite elements models: Anatomical model (AN); Simplified model (PA6).

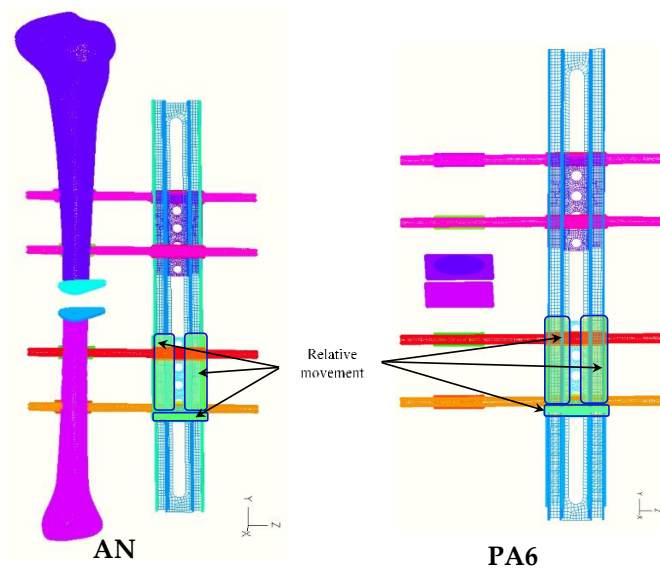


**Figure 5.** Contact surfaces included in the numerical models: Anatomical model (AN); Simplified model (PA6).

**Table 4.** Description of the total number of elements and nodes per model.

	Simplified	Anatomic
Elements	272075	373624
Nodes		

This study assumed isotropic linear elastic properties for all components, and their mechanical properties were those previously presented in Table 1. The loading, representing the electromechanical stimulus, was included by prescribing a 2 mm displacement at the holes of the free clamp, where the elongator was connected, as indicated in Figure 4.

### 3. Results

#### 3.1. Experimental Results

Figure 6 compares the results for the several types of Sawbones® (10, 15, 20, 30, 40, 50) blocks using the notation presented in Equation (1). The sawbones stiffness for the different blocks is shown in the graphic with the orange line; Figure 6a presents the results related to the simplified models, whereas Figure 6b presents those related to the anatomical model. The two sets of results showed that, as the stiffness of the osteotomy material increased, the displacement at the osteotomy decreased; hence, both lines show negative slopes.

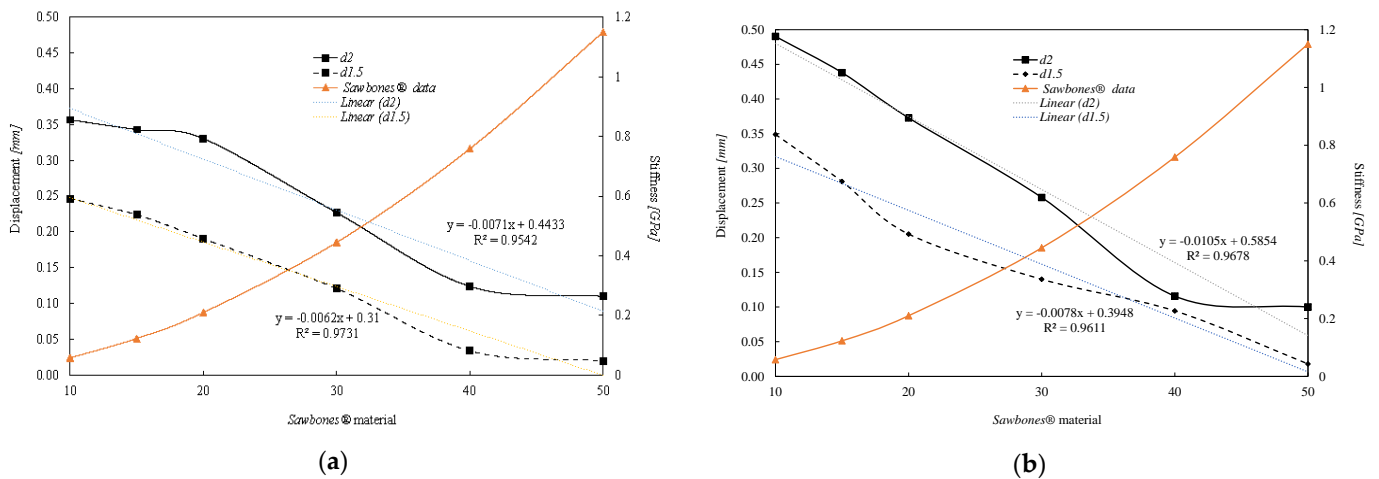


**Figure 6.** Displacement at the osteotomy in the two experimental models: (a) the simplified model; (b) the anatomical model.

Figure 6 shows that if the osteotomy material with the lower stiffness was under an imposed displacement of 2 mm through the worm screw, it received only 18% of the 2 mm. This percentage of displacement was calculated by comparing the displacement measured in osteotomy with the displacement imposed in the micromotor. Figure 7a compares the osteotomy displacement for the Sawbones® 20 material when three different values of prescribed displacement were defined at the worm screw of both fixator models. The behavior of both models was quite similar, and the differences were mainly related to the geometrical dimensions of the two models. Moreover, these results confirmed that, as the osteotomy's stiffness increased, the discharge of the force between the bone and the fixator was different, as described by several works [30–32]. Table 5 contains the values of Figure 7a and the prescribed displacement ratio measured at the osteotomy.

The tests carried out on the simplified and anatomical models allowed recording the energy consumption of the micromotor (CEMotor) in the variations of displacement versus stiffness at the osteotomy. Figure 7b shows the values of the CEMotor variable for the simplified and anatomy models to assure a prescribed displacement of 2 mm at the worm screw and using a 2 mm/min velocity.

Figure 7b allows the quantification of the CEMotor variable for several osteotomy stiffnesses. In the initial phase of healing, particularly, there was a higher increase in the stiffness and, simultaneously, in the value of the CEMotor variable. After this initial phase, the CEMotor variable showed a stabilization with slight variations.

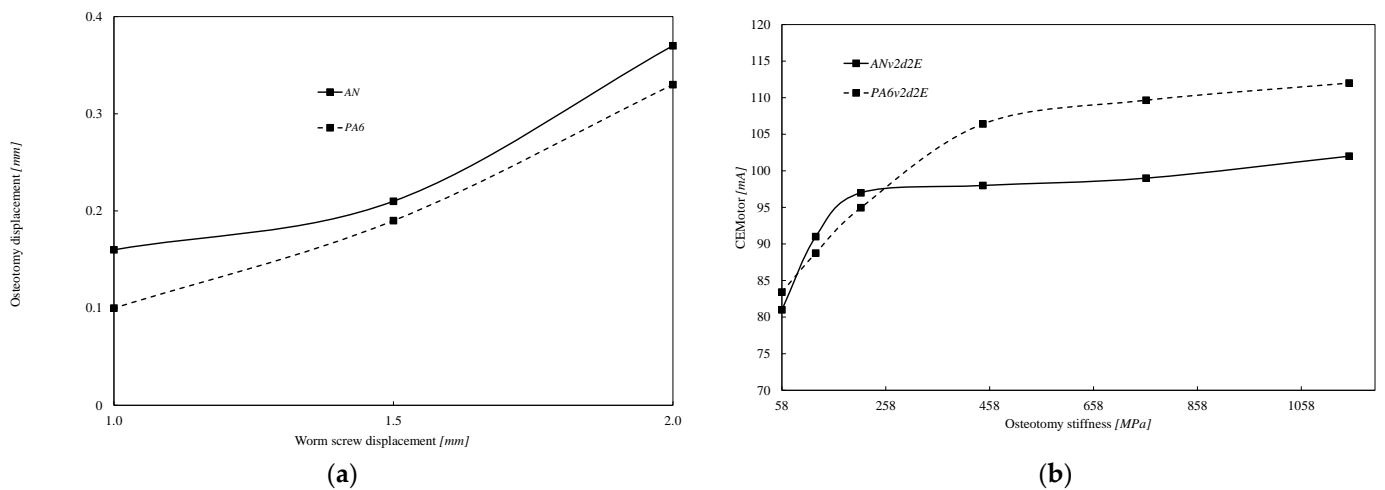


**Figure 7.** (a) Displacement at the osteotomy in the two experimental models using the Sawbones® 20 material at the osteotomy; (b) variation of CEMotor variable with the stiffness of the material at the osteotomy.

**Table 5.** Ratio of the prescribed displacements at the osteotomy for the Sawbones® 20 material.

Prescribed [mm]	PA6 Model		AN Model	
	Osteotomy [mm]	Ratio [%]	Osteotomy [mm]	Ratio [%]
2	0.33	17%	0.37	19%
1.5	0.19	13%	0.21	14%
1	0.1	10%	0.16	16%

### 3.2. Numerical Results

The simulations of the two models completed all time steps. The displacements over each axes directions and its magnitude were analyzed. The first analysis was based on the displacement distribution in the osteotomy when 2 mm of prescribed displacement were defined at the worm screw. Since the *y*-axis is parallel to the solicitation direction and the fixator axes, the average *y* displacements at the osteotomy face firstly loaded are presented in Table 6. The average values were evaluated considering all nodes of the osteotomy face of both models. In addition, the maximum displacement value on the same face is also presented. It is possible to observe that as the stiffness of the osteotomy material increased, the displacement decreased, with both models showing similar behavior.

**Table 6.** Average and maximum Y-displacement in the face of the osteotomy firstly loaded.

Osteotomy Material	PA6 Model [mm]		AN Model [mm]	
	Average	Maximum	Average	Maximum
S10	0.35	0.49	0.55	0.59
S15	0.30	0.43	0.48	0.52
S20	0.29	0.38	0.42	0.46
S30	0.20	0.29	0.30	0.34
S40	0.12	0.18	0.14	0.17
S50	0.11	0.16	0.11	0.14

For both models, Figures 8 and 9 show the distribution of *y*-displacement at the interface wherein the contact appeared firstly. The distribution pattern varied with the material’s stiffness. The homogeneity of the displacements increased as the osteotomy stiffness increased, suggesting that stimulation would be more challenging to implement as bone regeneration occurred. The image on the right-hand side of both figures shows the

view in the XZ plane, wherein it is possible to identify the Schanz pins, the cross section of the external fixator, and the two osteotomy geometries. In Figure 8, the osteotomy is represented by a block of Sawbones® material, while in Figure 9, it is defined by the anatomic tibia geometry. The maximum displacement magnitude value appeared in the same region for all the materials applied at the osteotomy. It was in the lateral zone closest to the fixator, as shown in Figure 10.

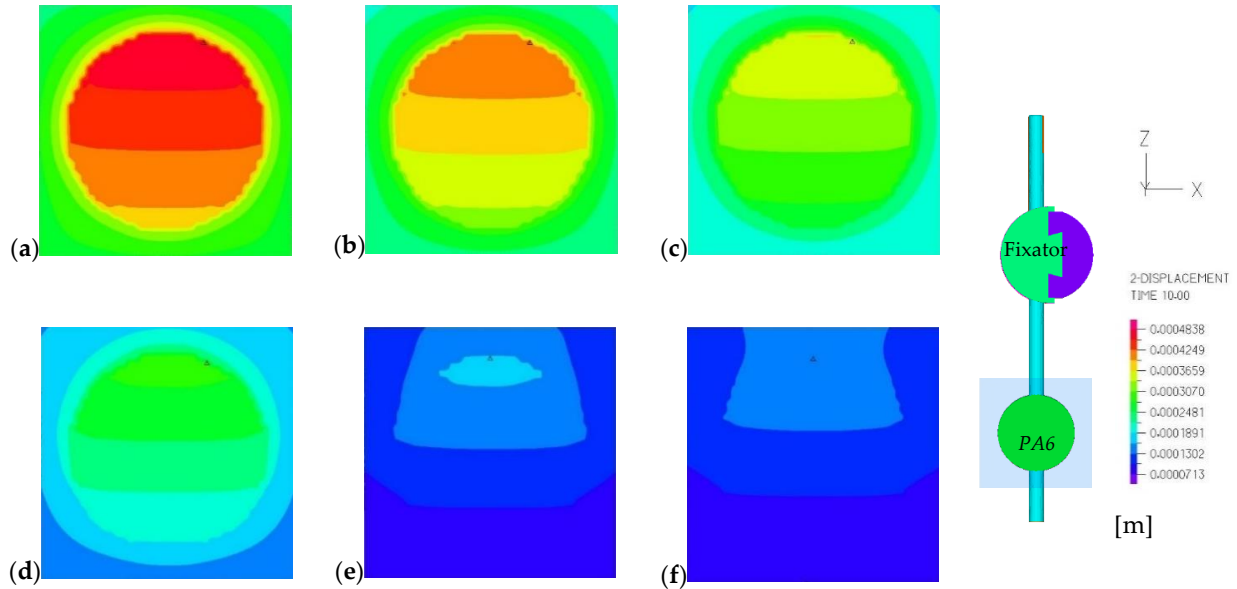


**Figure 8.** Distribution of Y displacement in the osteotomy surface of the PA6 model for a prescribed displacement of 2 mm and the following Sawbones® materials: (a) S10; (b) S15; (c) S20; (d) S30; (e) S40; (f) S50.

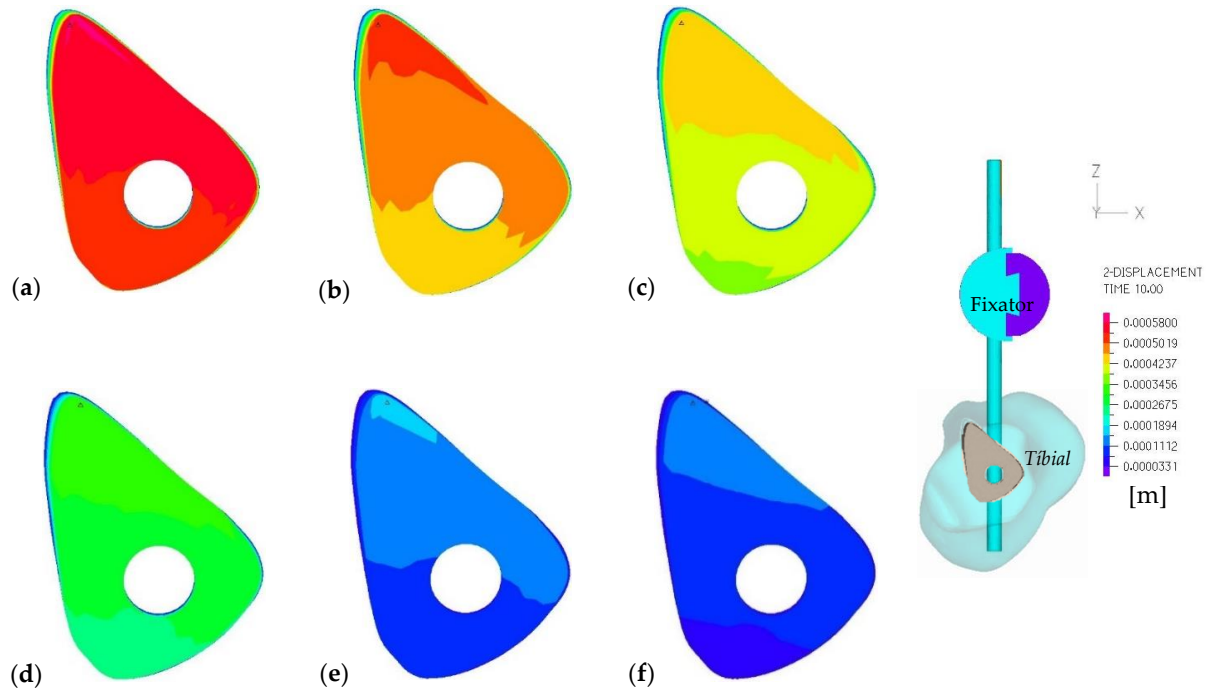


**Figure 9.** Distribution of Y displacement in the osteotomy surface of the AN model for a prescribed displacement of 2 mm and the following Sawbones® materials: (a) S10; (b) S15; (c) S20; (d) S30; (e) S40; (f) S50.

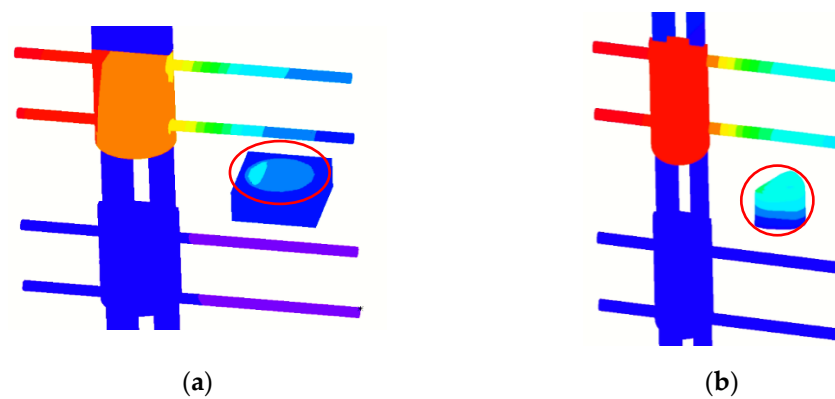


**Figure 10.** Localization of the maximum displacement magnitude value at the osteotomy on both models: (a) PA6; (b) AN.

The numerical simulation allowed understanding the biomechanical behavior of the assembly and, mainly, the mechanical behavior of the movable clamp. Hence, Figures 11 and 12 show the distribution of contact forces between the mobile clamp’s surface and the external fixator’s rail, indicating that they did not have a uniform distribution along the axis. This fact confirmed that transversal movements occurred in assembly, as suggested by some authors [16,20,33].

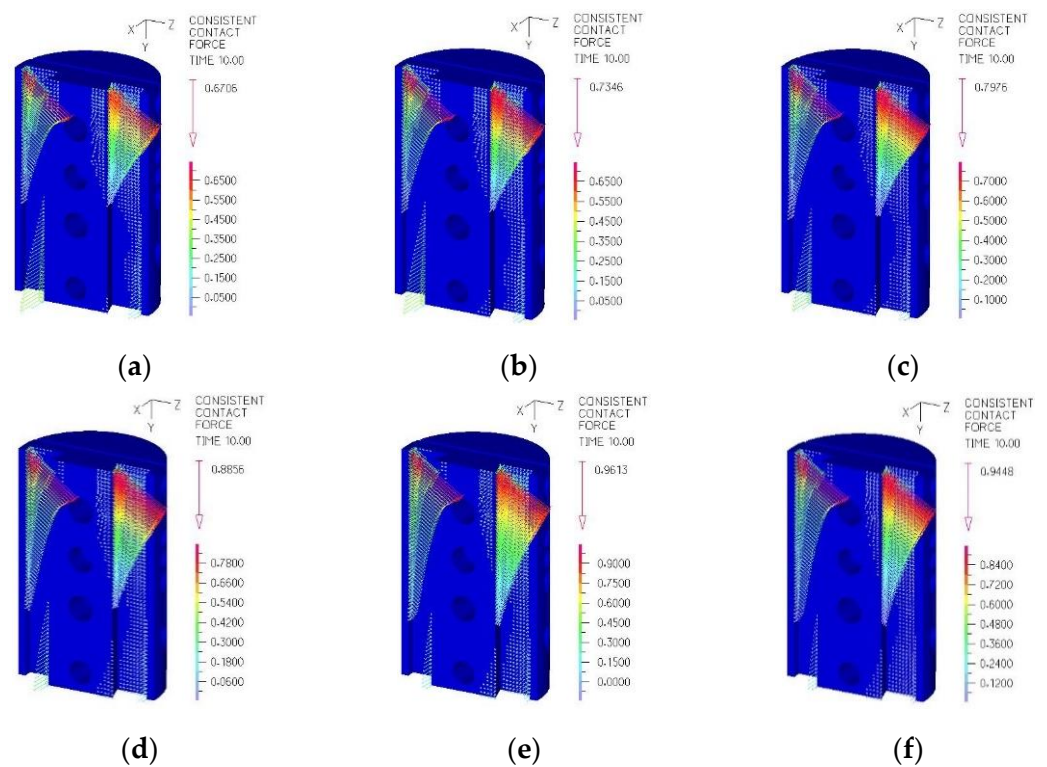


**Figure 11.** Distribution of contact forces in the movable clamp in the PA6 model for the following osteotomy materials: (a) S10; (b) S15; (c) S20; (d) S30; (e) S40; (f) S50.

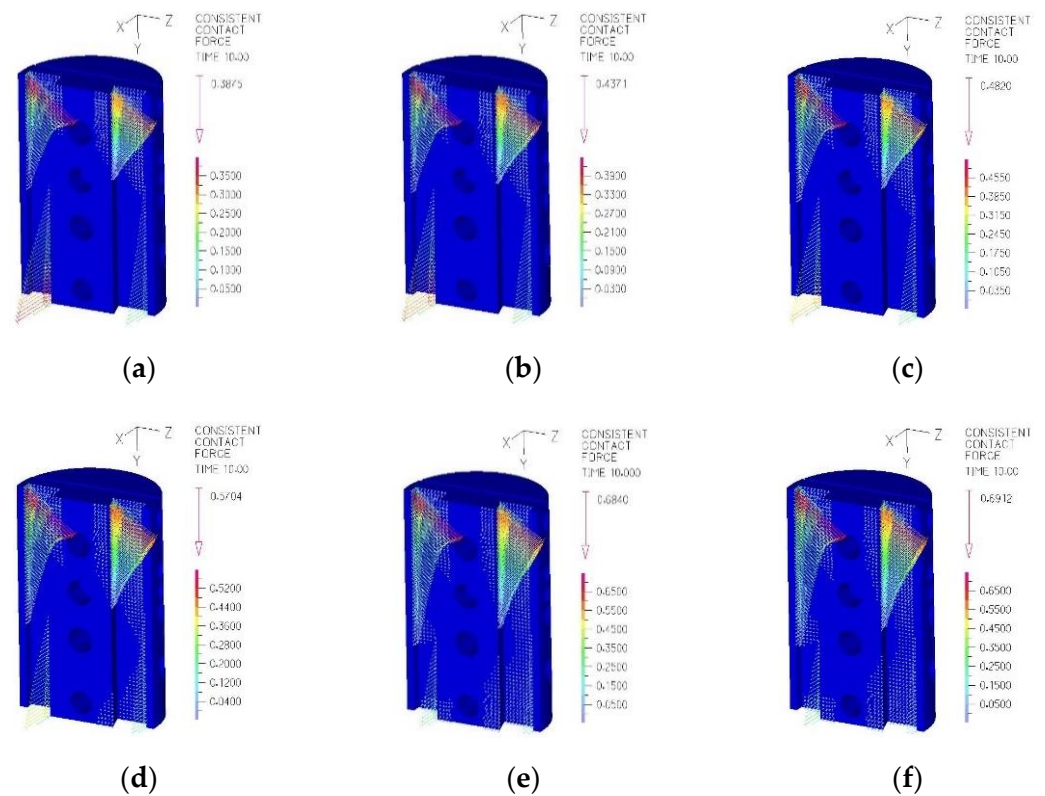


**Figure 12.** Distribution of contact forces in the movable clamp in the AN model for the following osteotomy materials: (a) S10; (b) S15; (c) S20; (d) S30; (e) S40; (f) S50.

The maximum values of the contact forces in all situations presented in Figures 11 and 12 are compiled in Table 7. In the PA6 model, the maximum value of contact forces between the movable clamp and the fixator rail for the Sawbones® 10 material was 0.671 N. Still, when the Sawbones® 40 material represented the osteotomy, the contact force increased to 0.961 N. The increase in the contact strength was proportional to the growth of stiffness, around 41%. In the anatomical model, the contact forces showed a similar distribution. However, when the stiffness of the osteotomy changed from the least to the most rigid material, the maximum value of contact force increased by about 78%.

**Table 7.** Maximum contact forces at the contact interface between the mobile clamp and the rail of the external fixator.

Osteotomy Material	Maximum Contact Force [N]	
	PA6 Model	AN Model
S10	0.671	0.388
S15	0.735	0.437
S20	0.798	0.482
S30	0.886	0.570
S40	0.961	0.684
S50	0.945	0.691

The pattern distribution of contact forces presented in Figures 11 and 12 is typical of a relative movement mainly in the loading direction (axial direction) and tends to move through the directions orthogonal to the loading, leading flexion, and torsion effects. Although these effects could be observed in both models, they were smaller in the anatomical model.

The maximum von Mises stresses occurred on the pins of the mobile clamp, and their distribution was very similar for all osteotomy materials. Figure 13 shows the stress distribution observed when using the Sawbones<sup>®</sup> 20 material in the osteotomy.

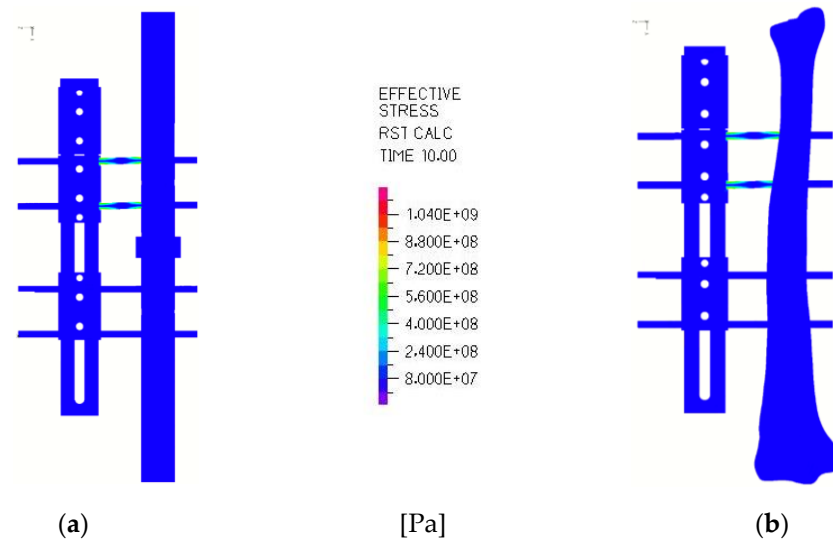


**Figure 13.** Effective stress in the numerical models  $S_{20d2}$ . (a) PA6; (b) AN.

It should be noted that, although the maximum effective stress had different values in the models, it always occurred in the pin closest to the osteotomy and the mobile clamp, as suggested by other authors [14].

#### 4. Discussion

The main purpose of this study was to contribute to the development of a technology able to promote callus stimulus and simultaneously predict bone fracture healing outcomes. The prototype was developed in the Orthofix<sup>®</sup> monoplane external fixation system, but the concept can be extended to another external fixation type where linear movement might occur. This technology is based on callus stiffness measurements that effectively diagnose and predict fracture healing outcomes [9,34–37]. Previous researchers have performed this attempt using strain gages on orthopedic plates [9,38,39], instrumented external fixators [34,40,41], and plates instrumented with telemetric sensors [37,42]; however, these techniques are, respectively, limited by the potential development of infection, limited hardware application, and impossibility to be used to promote direct callus stimulus.

This study demonstrated the possibility of establishing a relationship between energy consumption, CEMotor, by the electromechanical system used to perform callus stimulus, and the degree of osteotomy consolidation; this conclusion supports the idea of using the CEMotor variable to assess the state of callus growth. The electromechanical system can monitor the healing of regenerated bone or implement callus stimulation strategies of prescribing displacements to estimate callus consolidation and predict the removal of the external fixation system without additional diagnostic tests. Several studies that help support these conclusions have shown that the percentual mechanical load transferred to the osteotomy changes during the healing process [16,38,43] and that during acute healing (<30 days), the osteotomies progress to the proper union will exhibit a progressive improvement of mechanical strength. In contrast, this progression of increased osteotomy stiffness is arrested and/or delayed in those trending towards nonunion [36]. Moreover, in the biomechanical quantification of callus stiffness using indirect measurements, the load is shared between the fixation device and the bone [41]. Hence, if the fixator stiffness remains constant, the biomechanical quality of the callus formation is responsible for the measured data variation. The results of Figure 7b show that the stiffness of osteotomy was the main

reason for the CEMotor variable variation, which was high in the initial phase of “healing” and stabilized afterward.

Another point worth considering is related to callus stimulus. According to indications of the medical team, the introduction of loads with a view to micromovements can be performed between fibrous tissue and bone with immature stiffness [19,20,22]. Several researchers [24,44,45] suggest that bone callus stimulation of 1 mm (1000  $\mu\text{m}$ ) per day is beneficial to accelerate the healing process. The results of Table 4 show that the variation of the prescribed displacement at the elongator screw did not change the ratio of displacements for the same type of osteotomy material. Nevertheless, the osteotomy displacement was greater for Sawbones<sup>®</sup> materials with less rigidity. Still, when using materials with higher stiffness, the displacement in osteotomy was relatively reduced, which means that as the bone callus consolidated, the prescription of a constant 1 mm (1000  $\mu\text{m}$ ) displacement led to an increasingly small displacement of the osteotomy material.

Moreover, in Figure 6 is possible to identify the differences among the prescribed displacements and the displacements measured at the osteotomy, which can be used to estimate the percental load transferred to the callus [13]. The results showed that, because of the fastener distance, the friction, and the increase of the components in the assembly, it was impossible to reach the imposed displacement’s totality at the osteotomy. Furthermore, the results of Figure 6b indicate that in realistic situations, the prescription of stimulus displacements in the order of 1 mm (1000  $\mu\text{m}$ ) or 1.5 mm (1500  $\mu\text{m}$ ) can be interesting in the healing phase. Still, a higher stimulus displacement should be prescribed for bones with highly immature/mature stiffness. On the other hand, because the absolute value of the slope of the trendline related to the results of the prescribed displacement of 2 mm was higher than that of the 1.5 mm displacement, the anatomical model appeared to be more sensitive to variations of the osteotomy stiffness for higher prescribed values than for smaller ones. The results in Figure 6a show that the simplified model had a stiffer behavior than the anatomical model, especially for lower osteotomy stiffness values and smaller prescribed displacements. Nevertheless, the results of both models seemed to get closer for osteotomy stiffness values higher than 0.445 GPa and prescribed displacements in the order of 2 mm.

The predicted osteotomy displacements presented in Table 6 corroborated the experimental behavior, i.e., osteotomy displacements were more significant for Sawbones materials with less rigidity. The comparison between the experimental and the numerical results is presented in Table 8, wherein the results of Table 6 are also used to evaluate the relative error column.

**Table 8.** Comparison of experimental and numerical results of the osteotomy displacement.

Osteotomy Material	PA6 Model [mm]		AN Model [mm]	
	Experimental	Error [%]  (Exp-Num)/Exp	Experimental	Error [%]  (Exp-Num)/Exp
S10	0.36	3	0.49	13
S15	0.34	12	0.44	10
S20	0.33	13	0.37	12
S30	0.23	11	0.26	18
S40	0.12	3	0.12	17
S50	0.11	0.0	0.10	12

These results showed a good agreement, mainly in the simplified model (PA6), with a relative error lower than 13%; in the anatomical model, the relative error was higher, though it never reached 20%. Figures 8 and 9 show that the distribution pattern of the displacements at the osteotomy varied with the material’s stiffness and the distribution patterns of the two models were quite similar. Nevertheless, the anatomical models showed higher osteotomy compression values than the simplified tibia model, which can be corroborated by the differences of contact forces between the movable clamp and the

fixator rail in the two models, as presented in Table 7. The maximum von Mises stresses occurred on the pins of the mobile clamp, and their distribution was very similar for all osteotomy materials.

One of the limitations of this work is related to the lack of *in vivo* validation of the developed technology. In fact, despite the excellent quality of these results, the use of this technology for bone elongation and transport, wherein it is possible to evaluate all variables discretely, will help to understand the effect not only of several anatomic parameters on the CEMotor variable but also of other noncontrollable factors such as the variability of bone microstructure and mechanobiology among patients. Nevertheless, because this technology is mainly to monitor the CEMotor variable during the healing process in each patient and not among patients, it would be expected that these noncontrollable factors remain almost constant during the healing phase and that the biomechanical quality of the callus formation would be responsible for the measured data variation. Another limitation is related to some numerical modeling simplifications, such as the assumption of isotropic material instead of using bone orthotropic or transversely isotropic material [23]. Nevertheless, this assumption will mainly affect the level and distribution of strain and stress through the bone and, in a smaller scale, the global displacement and stiffness behavior.

According to the information from the medical team, after performing osteotomy (surgical) and, roughly, after 10 days from surgery, the patient should start daily stretching of approximately 1 mm (1000  $\mu\text{m}$ )/day. Thus, the patient must daily introduce a rotation movement in the elongator using a suitable wrench to promote the movement of the mobile clamp. Typically, this practice is performed in discrete steps four times a day (0.25 mm each) by the patient. In this way, implementing the electromechanical system in a more compact version can automate this procedure, guaranteeing a daily stretching in multiple discrete steps of smaller amplitude, which can be programmed and performed daily.

## 5. Conclusions

From this study, it is possible to build up the following consideration: to assure a proper mechanical stimulation of the osteotomy callus is important to account for the mechanical behavior of the external fixator used to do the stimulation procedure. One way of assuring this knowledge is to build experimental or numerical models that capture all mechanical components' main issues. In the case of the external fixator (Orthofix<sup>®</sup> LRS, Munich, Germany) used in this study, it was possible to show that the displacement in the osteotomy was always lower than the displacement prescribed in the elongator. However, it was possible to estimate a relationship that allows prescribed displacement adjustments to verify the intended displacement at the osteotomy. Moreover, the results of the electromechanical system developed may lead to methodologies of mechanical stimulation for regenerating bone, which will play a relevant role in the context of bedridden individuals with mobility limitations. Furthermore, a methodology based on this type of electromechanical system is expected to lead to a quick recovery, as it will allow more uniform healing.

**Author Contributions:** Conceptualization L.M.R. and A.M.A.; methodology M.F.P., L.M.R., I.B., M.A.N. and A.M.A.; software, M.F.P. and M.A.N.; validation, M.F.P., L.M.R., I.B., M.A.N. and A.M.A.; writing—original draft preparation, M.F.P., M.A.N. and A.M.A.; writing—review and editing, M.F.P., L.M.R., I.B., M.A.N. and A.M.A. All authors have read and agreed to the published version of the manuscript.

**Funding:** This research received no external funding.

**Institutional Review Board Statement:** Not applicable.

**Informed Consent Statement:** Not applicable.

**Data Availability Statement:** Not applicable.

**Acknowledgments:** This research was sponsored by national funds through FCT—Fundação para a Ciência e a Tecnologia, under the project UIDB/00285/2020.

**Conflicts of Interest:** The authors declare no conflict of interest.

## References

- Perren, S.M. Evolution of the internal fixation of long bone fractures. The scientific basis of biological internal fixation: Choosing a new balance between stability and biology. *J. Bone Joint Surg. Br.* **2002**, *84*, 1093–1110. [[CrossRef](#)] [[PubMed](#)]
- Cunningham, J. The biomechanics of fracture fixation. *Curr. Orthop.* **2001**, *15*, 457–464. [[CrossRef](#)]
- Hente, R.; Füchtmeier, B.; Schlegel, U.; Ernstberger, A.; Perren, S.M. The influence of cyclic compression and distraction on the healing of experimental tibial fractures. *J. Orthop. Res.* **2004**, *22*, 709–715. [[CrossRef](#)] [[PubMed](#)]
- Abulaiti, A.; Yilihamu, Y.; Yasheng, T.; Alike, Y.; Yusufu, A. The psychological impact of external fixation using the Ilizarov or Orthofix LRS method to treat tibial osteomyelitis with a bone defect. *Injury* **2017**, *48*, 2842–2846. [[CrossRef](#)] [[PubMed](#)]
- Yilihamu, Y.; Keremu, A.; Abulaiti, A.; Maimaiti, X.; Ren, P.; Yusufu, A. Outcomes of post-traumatic tibial osteomyelitis treated with an Orthofix LRS versus an Ilizarov external fixator. *Injury* **2017**, *48*, 1636–1643. [[CrossRef](#)] [[PubMed](#)]
- Chavoshnejad, P.; Ayati, M.; Abbaspour, A.; Karimpur, M.; George, D.; Rémond, Y.; Heidary Rouchi, A.; Baniassadi, M. Optimization of Taylor spatial frame half-pins diameter for bone deformity correction: Application to femur. *Proc. Inst. Mech. Eng. Part H J. Eng. Med.* **2018**, *232*, 673–681. [[CrossRef](#)] [[PubMed](#)]
- Kalinowski, A.; Linessio, R.P.; Mendonca, C.J.A.; Antunes, P.; Ramos, A.; Silva, J.C.C. Da Noninvasive Optical Instrumentation for Bone Healing Process Analysis. *IEEE Sens. J.* **2021**, *21*, 14060–14068. [[CrossRef](#)]
- Barcik, J.; Epari, D.R.; Ibrahim, T.; Mercatali, L.; Maria Donati, D. Can Optimizing the Mechanical Environment Deliver a Clinically Significant Reduction in Fracture Healing Time? *Biomedicines* **2021**, *9*, 691. [[CrossRef](#)]
- Ernst, M.; Richards, R.G.; Windolf, M. Smart implants in fracture care—Only buzzword or real opportunity? *Injury* **2021**, *52* (Suppl. 2), S101–S105. [[CrossRef](#)]
- Ledet, E.H.; Liddle, B.; Kradinova, K.; Harper, S. Smart implants in orthopedic surgery, improving patient outcomes: A review. *Innov. Entrep. Health* **2018**, *5*, 41. [[CrossRef](#)]
- Andreu-Perez, J.; Leff, D.R.; Ip, H.M.D.; Yang, G.Z. From Wearable Sensors to Smart Implants—Toward Pervasive and Personalized Healthcare. *IEEE Trans. Biomed. Eng.* **2015**, *62*, 2750–2762. [[CrossRef](#)] [[PubMed](#)]
- Lange, H.E.; Arbeiter, N.; Bader, R.; Kluess, D. Performance of a Piezoelectric Energy Harvesting System for an Energy-Autonomous Instrumented Total Hip Replacement: Experimental and Numerical Evaluation. *Materials* **2021**, *14*, 5151. [[CrossRef](#)] [[PubMed](#)]
- Duda, G.N.; Mandruzzato, F.; Heller, M.; Goldhahn, J.; Moser, R.; Hehli, M.; Claes, L.; Haas, N.P. Mechanical boundary conditions of fracture healing: Borderline indications in the treatment of unreamed tibial nailing. *J. Biomech.* **2001**, *34*, 639–650. [[CrossRef](#)]
- ASM International Handbook Committee. Properties and Selection: Nonferrous Alloys and Special-Purpose Materials. *ASM Int.* **1998**, *2*, 1143–1144.
- Silva, R. *Estudo Experimental Comparativo do Posicionamento dos Componentes Estruturais de um Fixador Externo*; University of Coimbra: Coimbra, Portugal, 2017.
- Martins Amaro, A.; Paulino, M.F.; Roseiro, L.M.; Neto, M.A.; Fátima Paulino, M.; Manuel Roseiro, L.; Augusta Neto, M. The Effect of External Fixator Configurations on the Dynamic Compression Load: An Experimental and Numerical Study. *Appl. Sci.* **2020**, *10*, 3. [[CrossRef](#)]
- Tan, E.S.; Mat Jais, I.S.; Rahim, S.A.; Tay, S.C. Effect of interfragmentary gap on compression force in a headless compression screw used for scaphoid fixation. *J. Hand Surg. Eur. Vol.* **2018**, *43*, 93–96. [[CrossRef](#)]
- Sawbones®. *Biomechanical Products Catalog*; Sawbones®: Limhamn, Sweden, 2019.
- Ghiasi, M.S.; Chen, J.E.; Rodriguez, E.K.; Vaziri, A.; Nazarian, A. Computational modeling of human bone fracture healing affected by different conditions of initial healing stage. *BMC Musculoskelet. Disord.* **2019**, *20*, 562. [[CrossRef](#)]
- Zhao, X.; Li, J.; Chen, Y.; Tao, C.; Ji, R. Investigation of load transfer process between external fixator and bone model by experimental and finite element methods. *J. Appl. Biomater. Funct. Mater.* **2019**, *17*, 2280800019826512. [[CrossRef](#)]
- Isaksson, H.; Wilson, W.; van Donkelaar, C.C.; Huijskes, R.; Ito, K. Comparison of biophysical stimuli for mechano-regulation of tissue differentiation during fracture healing. *J. Biomech.* **2006**, *39*, 1507–1516. [[CrossRef](#)]
- Lacroix, D.; Prendergast, P.J. A mechano-regulation model for tissue differentiation during fracture healing: Analysis of gap size and loading. *J. Biomech.* **2002**, *35*, 1163–1171. [[CrossRef](#)]
- Lopes, V.M.M.; Neto, M.A.; Amaro, A.M.; Roseiro, L.M.; Paulino, M.F. FE and experimental study on how the cortex material properties of synthetic femurs affect strain levels. *Med. Eng. Phys.* **2017**, *46*, 96–109. [[CrossRef](#)] [[PubMed](#)]
- Kenwright, J.; Richardson, J.B.; Cunningham, J.L.; White, S.H.; Goodship, A.E.; Adams, M.A.; Magnussen, P.A.; Newman, J.H. Axial movement and tibial fractures. A controlled randomised trial of treatment. *J. Bone Joint Surg. Br.* **1991**, *73*, 654–659. [[CrossRef](#)] [[PubMed](#)]
- Wehner, T.; Claes, L.; Niemeier, F.; Nolte, D.; Simon, U. Influence of the fixation stability on the healing time—a numerical study of a patient-specific fracture healing process. *Clin. Biomech.* **2010**, *25*, 606–612. [[CrossRef](#)] [[PubMed](#)]

26. Sigurdson, U.; Reikeras, O.; Utvag, S.E. The influence of compression on the healing of experimental tibial fractures. *Injury* **2011**, *42*, 1152–1156. [[CrossRef](#)] [[PubMed](#)]
27. Claes, L.; Augat, P.; Suger, G.; Wilke, H.J. Influence of size and stability of the osteotomy gap on the success of fracture healing. *J. Orthop. Res.* **1997**, *15*, 577–584. [[CrossRef](#)] [[PubMed](#)]
28. Miramini, S.; Zhang, L.; Richardson, M.; Mendis, P.; Ebeling, P.R. Influence of fracture geometry on bone healing under locking plate fixations: A comparison between oblique and transverse tibial fractures. *Med. Eng. Phys.* **2016**, *38*, 1100–1108. [[CrossRef](#)]
29. Gardner, T.N.; Evans, M.; Kenwright, J. The influence of external fixators on fracture motion during simulated walking. *Med. Eng. Phys.* **1996**, *18*, 305–313. [[CrossRef](#)]
30. Glatt, V.; Bartnikowski, N.; Quirk, N.; Schuetz, M.; Evans, C. Reverse Dynamization: Influence of Fixator Stiffness on the Mode and Efficiency of Large-Bone-Defect Healing at Different Doses of rhBMP-2. *J. Bone Joint Surg. Am.* **2016**, *98*, 677. [[CrossRef](#)]
31. Glatt, V.; Evans, C.H.; Tetsworth, K. A Concert between Biology and Biomechanics: The Influence of the Mechanical Environment on Bone Healing. *Front. Physiol.* **2017**, *7*, 678. [[CrossRef](#)]
32. Li, J.; Zhao, X.; Hu, X.; Tao, C.; Ji, R. A theoretical analysis and finite element simulation of fixator–bone system stiffness on healing progression. *J. Appl. Biomater. Funct. Mater.* **2018**, *16*, 115–125. [[CrossRef](#)]
33. Betts, D.C.; Müller, R. Mechanical Regulation of Bone Regeneration: Theories, Models, and Experiments. *Front. Endocrinol.* **2014**, *5*, 211. [[CrossRef](#)] [[PubMed](#)]
34. Hente, R.; Cordey, J.; Perren, S.M. In vivo measurement of bending stiffness in fracture healing. *Biomed. Eng. Online* **2003**, *2*, 8. [[CrossRef](#)] [[PubMed](#)]
35. Wehner, T.; Gruchenberg, K.; Bindl, R.; Recknagel, S.; Steiner, M.; Ignatius, A.; Claes, L. Temporal delimitation of the healing phases via monitoring of fracture callus stiffness in rats. *J. Orthop. Res.* **2014**, *32*, 1589–1595. [[CrossRef](#)] [[PubMed](#)]
36. McGilvray, K.C.; Unal, E.; Troyer, K.L.; Santoni, B.G.; Palmer, R.H.; Easley, J.T.; Demir, H.V.; Puttlitz, C.M. Implantable microelectromechanical sensors for diagnostic monitoring and post-surgical prediction of bone fracture healing. *J. Orthop. Res.* **2015**, *33*, 1439–1446. [[CrossRef](#)]
37. Wolynski, J.G.; Labus, K.M.; Easley, J.T.; Notaroš, B.M.; Ilić, M.M.; Puttlitz, C.M.; McGilvray, K.C. Diagnostic prediction of ovine fracture healing outcomes via a novel multi-location direct electromagnetic coupling antenna. *Ann. Transl. Med.* **2021**, *9*, 1223. [[CrossRef](#)]
38. Gadowski, B.C.; McGilvray, K.C.; Easley, J.T.; Palmer, R.H.; Santoni, B.G.; Puttlitz, C.M. Partial gravity unloading inhibits bone healing responses in a large animal model. *J. Biomech.* **2014**, *47*, 2836–2842. [[CrossRef](#)]
39. Tan, Y.; Hu, J.; Ren, L.; Zhu, J.; Yang, J.; Liu, D. A Passive and Wireless Sensor for Bone Plate Strain Monitoring. *Sensors* **2017**, *17*, 2635. [[CrossRef](#)]
40. Seide, K.; Weinrich, N.; Wenzl, M.E.; Wolter, D.; Jürgens, C. Three-dimensional load measurements in an external fixator. *J. Biomech.* **2004**, *37*, 1361–1369. [[CrossRef](#)]
41. Claes, L.E.; Cunningham, J.L. Monitoring the Mechanical Properties of Healing Bone. *Clin. Orthop. Relat. Res.* **2009**, *467*, 1964. [[CrossRef](#)]
42. Seide, K.; Aljudaibi, M.; Weinrich, N.; Kowald, B.; Jürgens, C.; Müller, J.; Faschingbauer, M. Telemetric assessment of bone healing with an instrumented internal fixator: A preliminary study. *J. Bone Jt. Surg.-Ser. B* **2012**, *94-B*, 398–404. [[CrossRef](#)]
43. Grasa, J.; Gómez-Benito, M.J.; González-Torres, L.A.; Asiaín, D.; Quero, F.; García-Aznar, J.M. Monitoring in vivo load transmission through an external fixator. *Ann. Biomed. Eng.* **2010**, *38*, 605–612. [[CrossRef](#)] [[PubMed](#)]
44. Goodship, A.E.; Kenwright, J. The influence of induced micromovement upon the healing of experimental tibial fractures. *J. Bone Joint Surg. Br.* **1985**, *67*, 650–655. [[CrossRef](#)] [[PubMed](#)]
45. Tufekci, P.; Tavakoli, A.; Dlaska, C.; Neumann, M.; Shanker, M.; Saifzadeh, S.; Steck, R.; Schuetz, M.; Epari, D. Early mechanical stimulation only permits timely bone healing in sheep. *J. Orthop. Res.* **2018**, *36*, 1790–1796. [[CrossRef](#)] [[PubMed](#)]